Chapter 12

Magnetohydrodynamics: Modeling of a Kinematic Dynamo

12.1. Introduction

12.1.1. *Generalities*

In this chapter, we are interested in the growth of an electromagnetic instability produced by the motion of an electrically conducting fluid. Let us take an initially non-zero magnetic field. Let us consider a stationary flow and assume that we can regulate the intensity of the flow without changing its geometry. We observe that the magnetic field is deformed by the flow. Let us suppose that subsequently the initial source of magnetic field is abruptly removed, two cases are then possible:

– either the magnetic intensity disappears over time. This is called magnetic diffusion;

– or the magnetic intensity does not decrease over time. This is then a dynamo instability[1].

Let us consider for example the case of the deformation of a uniform field by a fluid in rotation. In order to simplify the problem, the flow will be taken as a cylinder in rotation around its revolution axis [PAR 66] [WEI 66]. An initial field perpendicular to the rotation axis of the cylinder is chosen. The motion of the

---

Chapter written by Franck PLUNIAN and Philippe MASSÉ.

1 It can happen that the magnetic intensity increases only in the presence of an initial field and that once this is removed the magnetic intensity decreases. This is then a magnetic amplifier and not a dynamo instability [KOL 61].

cylinder generates an electric current density. This current density induces a magnetic field which is added to the initial field. If the cylinder rotation rate is constant, then the magnetic field reaches a stable state. The final configuration of the field depends on the cylinder rotation rate (Figure 12.1). For a high rotation rate (the 4th image in Figure 12.1), the magnetic field is expelled towards the periphery of the cylinder. If at a given moment the initial magnetic field is removed then the geometry of the deformed field persists, but its intensity dies out over the time. The body rotation is thus not a dynamo.

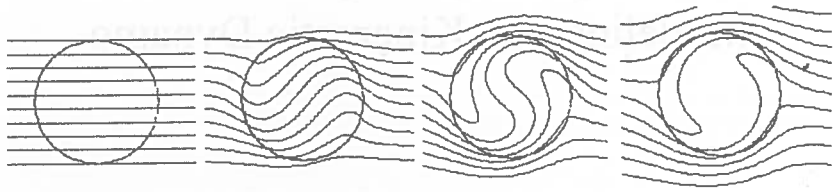

Figure 12.1. *Lines of magnetic field deformed by a cylinder in rotation (anti-clockwise direction). From left to right, rotation is increasing*

Now let us consider the preceding motion to which we add a velocity component in the direction of the axis of the cylinder (screw motion). The geometry of the magnetic field is then organized according to a double helix (Figure 12.2). Beyond a velocity threshold, the magnetic intensity grows over time even if removing the initial source of field. The screw motion is thus a dynamo.

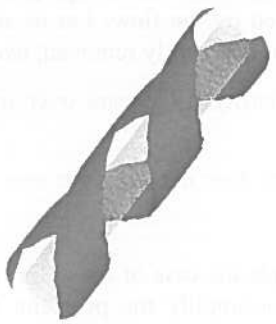

Figure 12.2. *Distribution of the magnetic energy generated by a screw motion [PLU 96]*

To know whether a flow is a dynamo or not, there is no general rule, except some anti-dynamo theorems [MOF 78] [HID 79] [PRO 79], which allows us to exclude flows which are too simple (e.g. 2D flows). Each flow must thus be the subject of a particular study.

Of course, it is actually impossible to regulate the flow intensity without changing its geometry. Indeed, starting at high velocity, the geometry of the flow cascades to smaller structures. The size of these structures, their distribution and their behavior evolve in a non-deterministic way (turbulent flow). In addition, even assuming that the flow is known and stationary, the magnetic intensity in the case of dynamo instability cannot increase indefinitely (according to the first principle of thermodynamics). Actually, the magnetic growth is accompanied by the feedback action of the magnetic field on the flow via Laplacian forces. Thus, in accordance with Lenz's law, the growth of the field is opposed to the fluid motion which generated it. The geometry of the flow, in theory, is thus modified by the dynamo instability. However, if we are interested in the appearance of the dynamo instability (zero growth rate) then the assumption of a geometry of flow determined *a priori* is relevant. In addition, even in the presence of a strongly turbulent fluid, we can in some cases consider only the average flow and show *a posteriori* that the turbulent fluctuations do not significantly influence the conditions of appearance of the dynamo effect [KRA 80]. Lastly, we have seen that the appearance of the dynamo instability requires a sufficiently vigorous flow (velocity threshold). Actually, a low flow rate can be compensated by the electric conductivity of the fluid, its magnetic permeability or by the characteristic scale of the flow. A dynamo flow can thus be, in theory, laminar or slightly turbulent, though it is not likely to happen in natural objects or experiments. When the geometry of the flow is considered known, the problem is called kinematic, in opposition to the dynamic problem which requires studying not only the evolution of the magnetic field but also that of the flow. In this chapter we limit ourselves to the study of the kinematic problem.

The kinematic theory of the dynamo effect [MOF 78] [ROB 92] helps us to understand the physics of magnetic field generation. Classes of dynamo have been identified: slow or fast dynamos, dynamos with scale separation (mean-field theory [KRA 80]) or not. Dynamo mechanisms have been identified: stretching, twisting, folding, shearing [CHI 95], alpha effect, etc. We will see some dynamo examples and their corresponding mechanisms.

The study of dynamo instability was born historically from the interest expressed in the origin of the magnetic field in the sun. It was extended to the majority of astrophysical objects (planets, stars, galaxies, etc.) [WEI 94] [RAD 95]. In fact, although the fluid contained in these objects is actuated by a relatively slow motion, the characteristic scales of the flow are so considerable that the dynamo effect is obtained almost systematically. Conversely, in the experiments undertaken in a

laboratory we try to compensate the relatively small characteristic dimension of the flow with a significant flow speed. In addition, it is for this reason that the dynamo effect is difficult to reproduce in a laboratory and does not have any practical or industrial application to date.

The major part of the solar magnetic field is in fact undetectable because it is hidden in the bottom of the convective zone. However, this part appears due to excursions out of the convective zone. These eruptions form arches on the surface of the sun (visible with the bare eye during an eclipse or with adapted optical instruments). They are at the origin of the sunspots. Additional evidence of solar magnetic activity is the dynamics of sunspots. These sunspots migrate towards the equator with a cycle of 22 years. Solar dynamo models try to reproduce the characteristics of this cycle (butterfly diagram) [PRI 82] [SCH 92]. On a larger time scale, the appearance of the sunspots is no longer cyclic but of a chaotic nature.

The dynamo effect is also at the origin of the terrestrial magnetic field. The nonlinear nature of the phenomenon is at the origin of the chaotic inversions of the magnetic dipole which paleomagneticians have highlighted by analyzing cooled lava or submarine sedimentary layers [COX 69] [MER 95] [VAL 93]. The electrically conducting fluid necessary for the geodynamo is the iron contained in the Earth's core. Its motion is of thermal origin. At the center, the liquid iron solidifies to form a solid inner core. This solidification is accompanied by the release of heat resulting in a natural convection mode of the liquid core.

Dynamo instability has also been the subject of theoretical [PLU 96] [PLU 98] [PLU 99] and experimental [ALE 00] studies in the liquid sodium cooling circuits of fast breeder reactors (FBR). In fact, the large volume of liquid sodium (electrically conducting) contained in the primary and secondary circuits, an appropriate flow geometry and a strong motion make FBR potential candidates for dynamo instability. In addition, if the steel used for the realization of the assemblies in which sodium circulates has a strong magnetic permeability (ferromagnetic steel), then dynamo instability is favored [PLU 95] [SOT 99].

Recently several research teams tried to reproduce a dynamo effect in a laboratory. Two experiments (also in liquid sodium) have been a success to date ([GAI 00] [GAI 01] [BUS 96] [RAD 98] [STI 01]). These are types of semi-dynamics experiments. Indeed, the flow forcing makes it possible to produce an average flow geometry quasi-independent of the forcing intensity on the one hand and of magnetic intensity on the other hand (similar to the kinematic context). Thus, above a certain threshold forcing power, magnetic energy increases exponentially. After a certain time, it is stabilized at a value depending on the intensity of forcing power. This balance results from the feedback action of the magnetic field on the flow intensity. The average flow is thus slowed down but its geometry is not

affected (or only slightly) as it would be it in a complete dynamic context. A second generation of experiments, dynamic experiments, is under study. Recently a third experiment has produced dynamo action within a strongly turbulent flow [MON 06]. In the nonlinear regime and for some parameters of the experiment, chaotic polarity reversals have been obtained [BER 07].

In this chapter, we are interested in modeling the kinematic dynamo effect using the finite element method. This enables us to determine the conditions of appearance of the dynamo instability for a given flow and to understand the physical mechanisms leading to this instability. The formulations which we present have been tested and validated. They have the advantage of being the least constraining possible (for example, at the level of electromagnetic property jumps) to allow discontinuities of electromagnetic properties. Since this chapter was written, other formulations have been proposed [LAG 06, GUE 07].

12.1.2. *Maxwell's equations and Ohm's law*

The usual electromagnetic quantities (magnetic field H, magnetic induction B, electric field E, current density J, electric charge q) have a behavior entirely described by:

– Maxwell's equations

$$\nabla\times(H)=j+\frac{\partial(\varepsilon E)}{\partial t}; \qquad \nabla\times(E)=-\frac{\partial(B)}{\partial t} \qquad [12.1]\ [12.2]$$

$$\nabla\cdot B=0; \qquad \nabla\cdot\varepsilon E=q; \qquad H=\frac{B}{\mu} \qquad [12.3]\ [12.4]\ [12.5]$$

– Ohm's law (expressed for a conducting fluid of velocity V)

$$j=\sigma(E+V\times B) \qquad [12.6]$$

μ, ε, σ and q being the magnetic permeability and permittivity, the conductivity and the electric charge respectively.

In the case of liquid metals, displacement currents $\partial(\varepsilon E)/\partial t$ are negligible with respect to j in [12.1]. Equation [12.1] is thus reduced to:

$$\nabla\times(H)=j \qquad [12.7]$$

In insulating zones ($\sigma = 0$), such as air, for example, [12.6] implies that there is no electric current j. It is thus deduced from [12.7] that H is derived from a gradient. In insulating zones, magnetic potential φ is thus defined by:

$$H=\nabla\varphi \qquad [12.8]$$

The conditions of continuity at two sub-domain interfaces are deduced from Maxwell's equations and Ohm's law:

$$[E\times n]=0\ ;\ [\sigma(E+V\times B)\cdot n]=0\ ;\ [B\cdot n]=0\ ;\ [H\times n]=0 \qquad [12.9a;b;c;d]$$

where n is defined as the normal vector directed towards the outside of the interface (I) or the border of the integration domain (Γ).

12.1.3. *The induction equation*

By combining equations [12.2], [12.5], [12.6] and [12.7] the induction equation is obtained:

$$\frac{\partial B}{\partial t}=\nabla\times(V\times B)-\nabla\times\left(\frac{1}{\sigma}\nabla\times\frac{B}{\mu}\right) \qquad [12.10]$$

It can be noted that [12.10] implies $\frac{\partial}{\partial t}(\nabla\cdot B)=0$. Relation [12.3] is thus an initial condition in time for B.

By performing the scalar product of [12.10] by B/μ, and while integrating on all the modeling space, we obtain:

$$\frac{\partial}{\partial t}\iiint_{(\Omega)}\frac{B^2}{2\mu}d\Omega+\oiint_{(\Gamma)}(E\times H)\cdot n dS+\iiint_{(\Omega)}(j\times B)\cdot V d\Omega+\iiint_{(\Omega)}\frac{j^2}{\sigma}d\Omega=0 \qquad [12.11]$$

The flux of the Poynting vector (2nd term) on a surface laid out *ad infinitum* is zero for the dynamo. Equation [12.11] thus expresses that the magnetic energy production (1st term) is possible provided that the work of the Laplacian forces (3rd term) is higher than dissipation by the Joule effect (4th term). This condition on the Laplacian forces requires a flow velocity of adequate geometry and of sufficiently high intensity. One of the difficulties of experimental reproduction devices is to find

a way of generating a flow whose geometry produces a dynamo effect at a reasonable speed.

12.1.4. *The dimensionless equation*

As often in physics, it is interesting to handle dimensionless equations whenever possible. In the case where σ and μ are constant in the flow, the induction equation is written:

$$\frac{\partial B}{\partial t'}=\nabla'\times(V'\times B)-R_m^{-1}\nabla'\times\left(\nabla'\times B\right) \qquad [12.12]$$

where R_m is the magnetic Reynolds number, defined by:

$$R_m=\sigma\mu VL \qquad [12.13]$$

The $'$ indicate dimensionless quantities, V and L the characteristic values of speed and length of the flow. For example, in the case of the Earth, L is the radius of the liquid core and V the characteristic speed of natural convection in the core. For the sun, L is the thickness of the convective zone. In Table 12.1, some orders of magnitude leading to the calculation of the magnetic Reynolds number (R_m) are presented for various natural objects [ZEL 83], for a fast breeder reactor as well as for the first two dynamo experiments carried out, one in Riga (Latvia), the other in Karlsruhe (Germany). The third experiment carried out in Cadarache (France) could achieve Rm=50 and the dynamo threshold was about 30 using ferromagnetic discs to produce the motion of liquid sodium (dynamo action was not obtained with stainless steel discs).

For a stationary flow (time independent), we show that the solution of induction equation [12.10] has the following form:

$$B(x,y,z,t)=\mathrm{Re}(B(x,y,z)e^{pt})$$

where p is a complex number. The real and imaginary parts of p are the growth rate and the pulsation of B respectively. The dynamo effect corresponds to $\mathrm{Re}(p)\geq 0$. The absence of dynamo is characterized by $\mathrm{Re}(p)\leq 0$ (diffusion). The complex parameter p depends on the geometry of the flow and on R_m.

	T K	L m	V $m\,s^{-1}$	ν m^2s^{-1}	ν_m m^2s^{-1}	R_e	R_m
Earth's core	$4\,10^3$	$35\,10^5$	$4\,10^{-4}$	10^{-6}	3	10^9	$5\,10^2$
Jupiter's core	10^4	$5\,10^7$	$5\,10^{-2}$	$3\,10^{-6}$	1	10^{12}	10^6
Convective zone of the sun	10^5	$2\,10^8$	10^3	$3\,10^{-5}$	10^3	$7\,10^{15}$	$2\,10^8$
Accretion disk around a black hole							
– interior area	$2\,10^6$	10^5	$5\,10^5$	$5\,10^2$	$1.5\,10^{-4}$	10^8	$3\,10^{13}$
– intermediate area	$3\,10^5$	10^6	$5\,10^3$	$3\,10^{-2}$	$4\,10^{-1}$	10^{11}	10^{10}
Interstellar environment							
– area HI	10^2	$3\,10^{17}$	$3\,10^3$	$2\,10^{15}$	$5\,10^{17}$	$5\,10^5$	$2\,10^3$
– area HII	10^4	$3\,10^{18}$	10^4	$5\,10^{14}$	$3\,10^{16}$	$5\,10^7$	10^6
– tunnel	10^6	$3\,10^{18}$	10^4	$3\,10^{22}$	$5\,10^{13}$	1	$6\,10^8$
Gas galactic disk	10^4	10^{19}	10^4	$5\,10^{13}$	10^{17}	$2\,10^9$	10^6
Universe in expansion	$4\,10^3$	$4\,10^{20}$	10^4	10^{13}	$5\,10^3$	$4\,10^{11}$	10^{21}
Fast breeder reactor	673	1	5.5	$7\,10^{-7}$	$2\,10^{-1}$	$8\,10^6$	25-30
Laboratory experiments							
– Riga	423	0.125	13	$6\,10^{-7}$	$8\,10^{-2}$	$3\,10^6$	20
– Karlsruhe	398	0.1	5	$7\,10^{-7}$	$8\,10^{-2}$	$7\,10^5$	6-7

Table 12.1. *Typical parameters of natural objects, industrial and experimental facilities leading to a dynamo effect*

For a given flow geometry, we can be interested for example in the minimum value of R_m, for which a dynamo effect occurs. This critical magnetic Reynolds number (R_m^c) corresponds to a zero growth rate ($Re(p)=0$).

For a given dynamo flow geometry, we can also be interested in the limit of $Re(p)$ when R_m tends towards infinity. Two classes of dynamo are thus defined, "slow" or "fast", depending on whether this limit is zero or not [CHI 95]. This distinction is relevant for many astrophysical objects (Sun, galaxy, etc.) for which R_m is very high ($>10^8$) and for which it is suitable to identify generation mechanisms compatible with such a value of R_m. In addition, the majority of astrophysical dynamo predictions is based on the mean field theory [KRA 80] and implicitly assumes the existence of fast dynamo.

The discretization according to space coordinates of the induction equation leads to a system of equations of the form $pB=M\cdot B$ where the matrix M depends on the

method of discretization (finite elements, Fourier series, finite differences, etc.) as well as on the discretization refinement (mesh size, number of Fourier modes, etc.). The possible values of p are thus the set of the eigenvalues of M. The significant growth rate p is thus the eigenvalue which has the largest real part. This eigenvalue can also be calculated using an appropriate temporal scheme of evolution of the equations and is physically measured in an experiment. In some cases, it is interesting to follow several eigenvalues according to the parameters of the problem [PLU 99].

12.2. Modeling the induction equation using finite elements

12.2.1. *Potential (A,ϕ) quadric-vector formulation*

12.2.1.1. *Definition of magnetic and scalar potentials*

The magnetic vector potential A and electric scalar potential ϕ are defined by:

$$B=\nabla\times A\,; \qquad E=-\nabla\phi-\partial A/\partial t \qquad [12.14]\ [12.15]$$

Any transformation of the form

$$A'=A+\nabla f\,; \qquad \phi'=\phi+\frac{\partial f}{\partial t} \qquad [12.16]\ [12.17]$$

where f is an unspecified scalar function changes neither E nor B. In order to ensure the unicity of the solution in quadri-vector (A,ϕ) it is necessary to impose a gauge condition which must be satisfied by (A,ϕ). The most current are the Coulomb and Lorenz gauges.

12.2.1.2. *Strong form*

Induction equation [12.10] can then also be formulated in vector and scalar potentials A and ϕ.

$$\nabla\times\left(\frac{\nabla\times A}{\mu}\right)=\sigma\left(-\frac{\partial A}{\partial t}-\nabla\phi+V\times\nabla\times A\right) \qquad [12.18]$$

Equation [12.18] is also valid for $\sigma=0$, unlike equation [12.10]. However, there is one more unknown variable than the number of equations to be solved. It is thus necessary to solve an additional equation which, logically, could result from the choice of gauge that potentials A and ϕ must check. However, we impose the Coulomb gauge:

$$\nabla \cdot A = 0 \qquad [12.19]$$

directly in the weak form of equation [12.18], using a least squares formulation [CSE 82]. This process has the advantage of symmetrizing the diffusion matrix but the disadvantage of no longer ensuring the continuity of the normal component of current density j at the interfaces. To overcome this disadvantage, we choose to solve the additional equation

$$0 = \nabla \cdot \left(\sigma \left(-\frac{\partial A}{\partial t} - \nabla \phi + V \times \nabla \times A \right) \right) \qquad [12.20]$$

This equation ensures in particular that $j_n = 0$ on an insulator. The expression of magnetic induction B is obtained thanks to equation [12.14]. Consequently, equation [12.3] is automatically checked. In order to again make the resolution matrices symmetric, the following change of variable is used [BIR 89]

$$\phi = \frac{\partial W}{\partial t} \qquad [12.21]$$

Finally the following system is solved

$$\begin{aligned} \nabla \times \left(\frac{\nabla \times A}{\mu} \right) &= \sigma \left(-\frac{\partial (A + \nabla W)}{\partial t} + V \times (\nabla \times A) \right) \\ \nabla \cdot \left(\sigma \left(-\frac{\partial (A + \nabla W)}{\partial t} + V \times (\nabla \times A) \right) \right) &= 0 \end{aligned} \qquad [12.22]$$

with gauge [12.19].

In addition to the continuity conditions at interfaces described by equations [12.9], it is necessary to add the continuity of the normal component of A:

$$[A \cdot n] = 0 \qquad [12.23]$$

12.2.1.3. *Weak form*

The weak form of the formulation in (A, W) is obtained by projecting equations [12.22] on the space of test functions (α, β).

$$\begin{aligned} &\iiint_{(\Omega)} \left(\frac{1}{\mu} \nabla \times \alpha \cdot \nabla \times A + \frac{1}{\mu} \nabla \cdot \alpha \cdot \nabla \cdot A + \sigma \alpha \cdot \left(\frac{\partial (A + \nabla W)}{\partial t} - V \times \nabla A \right) \right) d\Omega + \\ &\iint_{(I) \cup (\Gamma)} \left(-\frac{\nabla \cdot A}{\mu} (\alpha \cdot n) + \alpha \cdot \left(n \times \frac{\nabla \times A}{\mu} \right) \right) dS = 0 \end{aligned} \qquad [12.24a]$$

$$\begin{aligned} &\iiint_{(\Omega)} \left(\sigma \nabla \beta \cdot \left(\frac{\partial (A + \nabla W)}{\partial t} - V \times \nabla A \right) \right) d\Omega + \\ &\iint_{(I) \cup (\Gamma)} \sigma \beta \left(\frac{\partial (A + \nabla W)}{\partial t} + V \times \nabla A \right) dS = 0 \end{aligned} \qquad [12.24b]$$

This corresponds to the resolution of a matrix system $MX + L\frac{dX}{dt} = F(X)$ where X is the quadri-vector (A, W) and M and L the matrices defined with the usual notations by:

$$M_{11} = M_{22} = M_{33} = \mu^{-1} (\partial_x \alpha_i \cdot \partial_x \alpha_j + \partial_y \alpha_i \cdot \partial_y \alpha_j + \partial_z \alpha_i \cdot \partial_z \alpha_j) ;$$

$$M_{12} = \mu^{-1} (-\partial_y \alpha_i \cdot \partial_x \alpha_j + \partial_x \alpha_i \cdot \partial_y \alpha_j) ; \; M_{13} = \mu^{-1} (-\partial_z \alpha_i \cdot \partial_x \alpha_j + \partial_x \alpha_i \cdot \partial_z \alpha_j) ;$$

$$M_{21} = \mu^{-1} (-\partial_x \alpha_i \cdot \partial_y \alpha_j + \partial_y \alpha_i \cdot \partial_x \alpha_j) ; \; M_{23} = \mu^{-1} (-\partial_z \alpha_i \cdot \partial_y \alpha_j + \partial_y \alpha_i \cdot \partial_z \alpha_j) ;$$

$$M_{31} = \mu^{-1} (-\partial_x \alpha_i \cdot \partial_z \alpha_j + \partial_z \alpha_i \cdot \partial_x \alpha_j) ; \; M_{32} = \mu^{-1} (-\partial_y \alpha_i \cdot \partial_z \alpha_j + \partial_z \alpha_i \cdot \partial_y \alpha_j) ;$$

$$M_{14} = M_{24} = M_{34} = M_{41} = M_{42} = M_{43} = M_{44} = 0 ;$$

$$L_{11} = L_{22} = L_{33} = \sigma \alpha_i \cdot \alpha_j ; \; L_{12} = L_{13} = L_{21} = L_{23} = L_{31} = L_{32} = 0 ;$$

$$L_{14} = \sigma \alpha_i \cdot \partial_x \alpha_j ; \; L_{24} = \sigma \alpha_i \cdot \partial_y \alpha_j ; \; L_{34} = \sigma \alpha_i \cdot \partial_z \alpha_j ;$$

$$L_{41} = \sigma \partial_x \alpha_i \cdot \alpha_j ; \; L_{42} = \sigma \partial_y \alpha_i \cdot \alpha_j ; \; L_{43} = \sigma \partial_z \alpha_i \cdot \alpha_j ;$$

$$L_{44} = \sigma (\partial_x \alpha_i \cdot \partial_x \alpha_j + \partial_y \alpha_i \cdot \partial_y \alpha_j + \partial_z \alpha_i \cdot \partial_z \alpha_j) .$$

We can show that this formulation also corresponds to the minimization of equation [12.11] while taking $\alpha = \frac{\partial A}{\partial t}$ and $\beta = W$.

12.2.1.4. *Validity domain of the formulation*

The principal advantage of the formulation in quadri-vector potential with Coulomb gauge is its domain of validity. In particular:

– discontinuities of σ and μ are authorized;

– the conductors can be not simply connected;

– magnetic permeability μ can be nonlinear and anisotropic;

– the formulation is compatible with the modeling of the magnets.

However, if the integration domain is of constant magnetic permeability, then a more economic formulation in computer power can be used. In the non-conducting part, B being derived from a potential φ it is enough to calculate this potential (only one unknown variable). In the conducting part the calculation of B (3 unknown variables) is also enough. The saving in calculation time compared to the quadri-vector potential formulation can be significant. It is the object of the formulation in (B, φ) which we will not detail in this chapter; see [LAG 06] [GUE 07].

12.2.2. *2D$^{1/2}$ quadri-vector potential formulation*

12.2.2.1. *Strong form*

In the particular case where V, σ and μ are independent of one coordinate, for example of z in Cartesian coordinates, we then have an easy way of making it possible to reduce the previous problem to the resolution of a 2D problem [SOT 98] [SOT 99]. Let us consider the decomposition of the quadri-vector potential in Fourier series with respect to z

$$(A,W)=\sum_k (A_k,W_k)(x,y,t)e^{ikz} \qquad [12.25]$$

It is shown that the complex Fourier modes (A_k,W_k) are independent of each other. We thus solve a 2D problem depending only on x, y and t for each mode k.

The strong form of the 2D$^{1/2}$ complex quadri-vector potential formulation (A_k,ϕ_k) is thus written:

$$\nabla^*\times\left(\frac{\nabla^*\times A_k}{\mu}\right)=\sigma\left(-\frac{\partial(A_k+\nabla^* W_k)}{\partial t}+V\times(\nabla^*\times A_k)\right)$$
$$\nabla^*\cdot\left(\sigma\left(-\frac{\partial(A_k+\nabla^* W_k)}{\partial t}+V\times(\nabla^*\times A_k)\right)\right)=0 \qquad [12.26]$$

where operator ∇^* is defined by $\left(\frac{\partial}{\partial x},\frac{\partial}{\partial y},ik\right)$.

The Coulomb gauge is written

$$\nabla^*\cdot A_k=0 \qquad [12.27]$$

12.2.2.2. *Weak form*

The weak form of the 2D$^{1/2}$ complex quadri-vector potential formulation (A_k,ϕ_k) is obtained by projecting equations [12.26] on the space of the complex test functions (α_k,β_k).

$$\iint_{(\Omega^2)}\left(\frac{1}{\mu}(\nabla^*\times\alpha_k)\cdot(\nabla^*\times A_k)+\frac{1}{\mu}(\nabla^*\cdot\alpha_k)(\nabla^*\cdot A_k)+\sigma\alpha_k\cdot\left(\frac{\partial(A_k+\nabla^* W_k)}{\partial t}-V\times\nabla^*\times A_k\right)\right)d\Omega^2$$
$$\oint_{\Gamma^1\cup\Gamma^1}\left(\frac{\nabla^*\cdot A_k}{\mu}(\alpha_k\cdot n)+\alpha_k\cdot\left(n\times\frac{\nabla^*\times A_k}{\mu}\right)\right)dl=0 \qquad [12.28a]$$

$$\iint_{(\Omega^2)}\left(\sigma\nabla^*\beta_k\cdot\left(\frac{\partial(A_k+\nabla^* W_k)}{\partial t}-V\times\nabla^* A_k\right)\right)d\Omega^2+$$
$$\int_{\Gamma^1\cup\Gamma^1}\sigma\beta_k\left(-\frac{\partial(A_k+\nabla^* W_k)}{\partial t}+V\times\nabla^* A_k\right)dS=0 \qquad [12.28b]$$

The weak form of [12.27] is solved again by the least squares method and corresponds to the second term of [12.28a]. Weak formulation [12.28] corresponds to the resolution of a matrix system $MX_k+L\frac{dX_k}{dt}=F(X_k)$ where X_k is the complex quadri-vector (A_k,ϕ_k), M and L the complex matrices defined with the usual notations by:

$$M_{11}=M_{22}=M_{33}=\mu^{-1}(\partial_x\alpha_i\cdot\partial_x\alpha_j+\partial_y\alpha_i\cdot\partial_y\alpha_j+k^2\alpha_i\cdot\alpha_j);$$
$$M_{12}=\mu^{-1}(-\partial_y\alpha_i\cdot\partial_x\alpha_j+\partial_x\alpha_i\cdot\partial_y\alpha_j);\ M_{13}=ik\mu^{-1}(\alpha_i\cdot\partial_x\alpha_j+\partial_x\alpha_i\cdot\alpha_j);$$
$$M_{21}=\mu^{-1}(-\partial_x\alpha_i\cdot\partial_y\alpha_j+\partial_y\alpha_i\cdot\partial_x\alpha_j);\ M_{23}=ik\mu^{-1}(\alpha_i\cdot\partial_y\alpha_j+\partial_y\alpha_i\cdot\alpha_j);$$
$$M_{31}=-ik\mu^{-1}(\partial_x\alpha_i\cdot\alpha_j+\alpha_i\cdot\partial_x\alpha_j);\ M_{32}=-ik\mu^{-1}(\partial_y\alpha_i\cdot\alpha_j+\alpha_i\cdot\partial_y\alpha_j);$$
$$M_{14}=M_{24}=M_{34}=M_{41}=M_{42}=M_{43}=M_{44}=0;$$
$$L_{11}=L_{22}=L_{33}=\sigma\alpha_i\cdot\alpha_j;\ L_{12}=L_{13}=L_{21}=L_{23}=L_{31}=L_{32}=0;$$
$$L_{14}=\sigma\alpha_i\cdot\partial_x\alpha_j;\ L_{24}=\sigma\alpha_i\cdot\partial_y\alpha_j;\ L_{34}=ik\sigma\alpha_i\cdot\alpha_j;$$

$$L_{41}=\sigma\partial_x\alpha_i\cdot\alpha_j\ ;\ L_{42}=\sigma\partial_y\alpha_i\cdot\alpha_j\ ;\ L_{43}=-ik\sigma\alpha_i\cdot\alpha_j\ ;$$
$$L_{44}=\sigma(\partial_x\alpha_i\cdot\partial_x\alpha_j+\partial_y\alpha_i\cdot\partial_y\alpha_j+k^2\alpha_i\cdot\alpha_j)\ .$$

12.2.2.3. *Validity domain of the formulation*

The validity domain of the $2D^{1/2}$ complex quadri-vector potential formulation is the same as for the 3D formulation, but with the limitation due to the reduction of the dimension of the integration domain:

– discontinuities of σ and μ are allowed only in plane (x,y);

– the conductors can be not simply connected in plane (x, y);

– magnetic permeability μ can be nonlinear and anisotropic in plane (x,y);

– the formulation is compatible with the modeling of the magnet formulation.

12.2.2.4. *Other $2D^{1/2}$ formulations*

The case where V, σ and μ are independent of the azimuthal component θ in cylindrical coordinates corresponds to another $2D^{1/2}$ formulation. The quadri-vector potential decomposition in Fourier series with respect to θ is thus considered:

$$(A,W)=\sum_m(A_m,W_m)(r,z,t)e^{im\theta} \qquad [12.29]$$

It is shown that the complex Fourier modes (A_m,W_m) are independent of each other. A 2D problem is thus solved depending only on r, z and t for each mode m. The strong and weak forms of this formulation are stated in the same way as for the formulation in z while operator ∇^* is defined by $\nabla^*=\nabla_{r,z}+i\frac{m}{r}\hat{e}_\theta$.

In the cases where V, σ and μ are independent of both z and θ cylindrical coordinates, a new formulation can be stated. The quadri-vector potential decomposition in Fourier series with respect to z and θ is thus considered:

$$(A,W)=\sum_{k,m}(A_{k,m},W_{k,m})(r,t)e^{i(m\theta+kz)} \qquad [12.30]$$

It is shown that complex Fourier modes $(A_{k,m},W_{k,m})$ are independent of each other. A 1D problem is thus solved depending only on r and t for each couple (k, m). The strong and weak forms of this formulation are stated in the same way as for the formulation in z while operator ∇^* is defined by $\nabla^*=\nabla_r+i\frac{m}{r}\hat{e}_\theta+ik\hat{z}$.

The previous $2D^{1/2}$ formulations in z, $2D^{1/2}$ in θ as well as the 1D formulation in quadri-vector potential can be also stated for formulation (B,φ). For the 1D formulation, the use of appropriate Bessel functions as test functions reduces the resolution domain to the conducting part only, saving computer power [MAR 06] [PEY 07].

12.3. Some simulation examples

12.3.1. *Screw dynamo (Ponomarenko dynamo)*

12.3.1.1. *Modeling*

The screw dynamo was initially solved by Ponomarenko [PON 73] and from then on has defined a dynamo benchmark in cylindrical geometry. It has since been studied with the aim of producing an experimental dynamo [GAI 76]. The experimental results obtained are in very good agreement with theoretical predictions [GAI 00] [GAI 01].

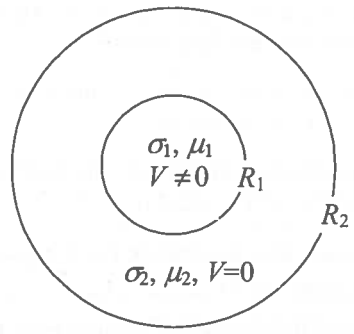

Figure 12.3. *Geometry of the integration domain for the screw dynamo*

Let us consider an integration domain composed of two parts with symmetry of revolution (Figure 12.3), which are coaxial and of height H:

– a cylinder with a radius R_1, a conductivity σ_1, a permeability μ_1 and a velocity $(V_r,V_\theta,V_z)=(0,\omega r,\chi\omega R_1)$;

– an external crown of radius $R_2>>R_1$, conductivity σ_2, permeability μ_2 and which is at rest (zero velocity).

Non-viscous screwing ($\omega = \omega_0$) is distinguished from viscous screwing (ω is dependent on r and becomes zero for $r=R_1$). The magnetic Reynolds number is

defined on the basis of characteristics of the moving inner-cylinder: $R_m=\sigma_1 \mu_1 \omega R_1^2 \sqrt{1+\chi^2}$. Since the motion is independent of θ and z, this problem can be described alternatively using a 3D, $2D^{1/2} ikz$, $2D^{1/2} im\theta$ or $1D ikz+im\theta$ formulation (section 12.2.2.3). It is thus possible to test and compare the various formulations while taking $H=\frac{2\pi}{k}=2\pi\chi R_1$ and periodic boundary conditions in $z=0$ and $z=H$ for the 3D and $2D^{1/2} im\theta$ modeling. The boundary conditions at the external domain border ($r=R_2$) can be Dirichlet or Neumann. This border is taken sufficiently far away from the conducting part ($R_2 \geq 10 R_1$) in order to be able to compare the numerical results with those obtained for ($R_2 \to +\infty$) by other methods. The initial condition must be non-zero and sufficiently complicated to contain the germ of the mode which will be amplified. An initial white noise condition type is sufficient.

12.3.1.2. *Main results*

– The screw motion is a dynamo with R_m^c depending on m, k, χ μ_2/μ_1 and σ_2/σ_1.

– The time evolution of the magnetic energy is exponential in accordance with the theoretical predictions for a stationary flow.

– In the homogenous case ($\mu_2/\mu_1=\sigma_2/\sigma_1=1$), the minimum value of R_m^c is 17.73. This is obtained for χ = 1.3, k=-0.39 and m=1.

– In the non-homogenous case, the results obtained for $\mu_2/\mu_1=a$ and $\sigma_2/\sigma_1=b$ are the same as those obtained for $\mu_2/\mu_1=b$ and $\sigma_2/\sigma_1=a$.

– For $R_m \geq R_m^c$, the larger R_m, the higher the dominant mode (m, k) (the mode which has the maximum growth rate).

– For viscous screwing, the maximum growth rate $\mathrm{Re}(p)=O(R_m^{-1/3})$ is obtained for $m,k=O(R_m^{1/3})$. The fact that $\mathrm{Re}(p)\to 0$ when $R_m \to +\infty$ confers its "slow" dynamo nature [GIL 88] [CHI 95] to viscous screwing. The maximum of magnetic energy is confined in a layer of a thickness $R_1 O(R_m^{-1/3})$.

– For non-viscous screwing, and for a given azimuth mode m, the maximum growth rate $\mathrm{Re}(p)=O(R_m^{-1/3})$ is obtained for $k=O(R_m^{1/2})$ also suggesting a "slow" dynamo action. However, this maximum growth rate according to k depends on m and reaches a maximum for $m=O(R_m^{1/2})$. This maximum, according to k and m, is $\mathrm{Re}(p)=O(1)$ for large R_m, conferring the "fast" nature of the non-viscous screwing dynamo [GIL 88] [CHI 95]. The maximum of magnetic energy is confined in a layer of thickness $R_1 O(R_m^{-1/2})$.

The neutral curves (zero growth rate) according to k and R_m are represented in Figure 12.4 for several ratios of different conductivity and permeability.

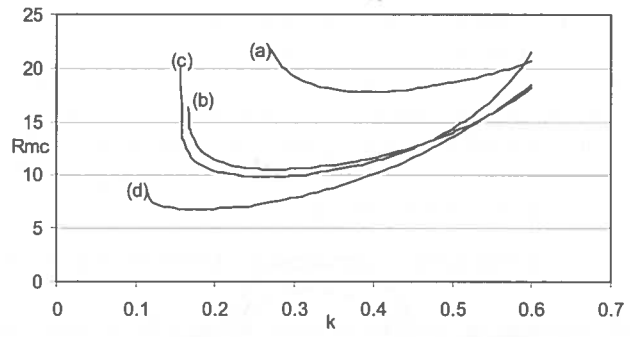

Figure 12.4. *Non-viscous Ponomarenko dynamo, m=1. The critical magnetic Reynolds number R_m^c is represented versus the vertical wave number k, for various electromagnetic properties. (a)$\sigma_2/\sigma_1=\mu_2/\mu_1=1$; (b) $\sigma_2/\sigma_1=10, \mu_2/\mu_1=1$; (c)$\sigma_2/\sigma_1=100, \mu_2/\mu_1=1$; (d)$\sigma_2/\sigma_1=\mu_2/\mu_1=10$. There is a dynamo action for $R_m \geq R_m^c$*

12.3.1.3. *Generation mechanism*

The field generation mechanism (for both viscous and non-viscous screwing) can be divided into two main phases: stretching by the flow shear and diffusion of the magnetic field lines.

In order to understand the stretching phase, it is necessary to first consider the case of a perfectly conducting fluid. It is thus shown that by stretching a magnetic flux tube, the magnetic intensity in the tube increases [MOF 78, MOR 90, CHI 95]. It is thus understood that the stretching related to the velocity gradients is a necessary ingredient for the dynamo effect. This ingredient is common to any dynamo flow, even if the fluid is not perfectly conducting. Here the magnetic field stretching results from a double shear: the one of the horizontal flow component (rotation) and the one of the vertical flow component. Due to the cylinder rotation, the magnetic field is stretched and deformed as represented in Figure 12.5.

Due to the stretching the magnetic field intensity increases. We also observe that the magnetic field lines are folded by the cylinder rotation. This folding implies that the magnetic field has opposite signs at the cylinder boundary. Therefore for pure rotation, these opposite field lines would cancel by diffusion (implying that pure rotation is not a dynamo flow). Let us consider now the shear between the cylinder vertical motion and the outer domain at rest. This shear has the effect (in addition to a stretching effect) to pull up the magnetic inner field at a height z different from the initial field and then constitutes the double helix of Figure 6.2. This magnetic double helix has also been observed experimentally [ALE 00]. The magnetic field after stretching is then mainly azimuthal and axial, approximately aligned with the

velocity shear. This constitutes the main part of the dynamo mechanism: the generation of a helical magnetic field from an initial radial field. To close the mechanism, we need this helical field to generate a radial field. This is done owing to diffusion of the azimuthal component of the helical field. Indeed, writing the magnetic diffusion in cylindrical coordinates clearly indicates that the diffusion of the azimuthal component occurs not only along the azimuthal coordinate but also along the radial coordinate (for non-zero m).

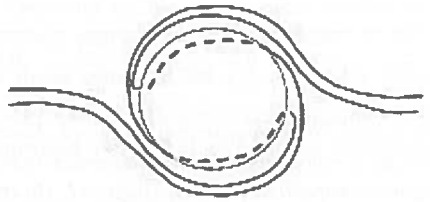

Figure 12.5. *Deformation of field lines by the cylinder rotation*

This heuristic explanation for the azimuth mode m=1 allows the characteristic mechanisms of a "slow" dynamo to be understood. Indeed, the diffusion plays a major part in the final arrangement of the magnetic field lines. It is shown that for $R_m \to +\infty$, the growth rate for m=1 tends towards zero. That is also true for any value of m. However, if we consider an infinite spectrum of azimuth modes m, then we show that in the case of non-viscous screwing, the dynamo is "fast" (Figure 12.6).

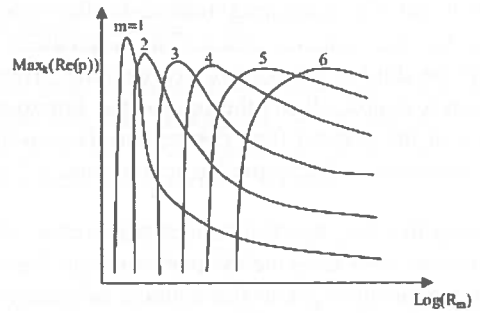

Figure 12.6. *Non-viscous Ponomarenko dynamo. The maximum according to the vertical wave number k of the growth rate Re(p), versus Log (Rm) and for various values of the azimuth wave number m. For given m, $Max_k(Re(p))$ tends towards zero with large R_m. On the other hand, the maximum according to k and m of Re(p) tends towards a non-zero value with large R_m*

12.3.2. *Two-scale dynamo without walls (Roberts dynamo)*

12.3.2.1. *Modeling*

Let us consider an integration domain made up of a square with side 2π and boundary conditions periodic in x and y. The flow is defined in dimensionless Cartesian coordinates by:

$$(V_x, V_y, V_z) = (\sin x \cos y, -\cos x \sin y, \sqrt{2}\chi \sin x \sin y)$$

This flow consists of parallel vortices moving in opposite directions. Each vortex is included in a cell of square section and the horizontal velocity is at maximum on the edges (Figure 12.7). The fluid is homogenous in electric conductivity and magnetic permeability. This problem was solved initially by G.O. Roberts [ROB 72] and from then on has defined a dynamo benchmark in Cartesian geometry. In addition, it has been studied with the aim of producing an experimental dynamo [BUS 96] [RAD 98]. The experimental results obtained [STI 01] are in good agreement with the theoretical predictions.

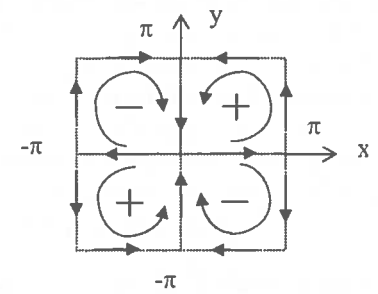

Figure 12.7. *Current lines of the Roberts flow in the xy plane. They coincide with the iso-values of V_z. The signs + (-) correspond to V_z>0 (<0)*

Since the motion is independent of z, this problem can be described alternatively using a 3D or $2D^{1/2}$ *ikz* formulation (section 12.2.2.3). This thus allows the various formulations to be tested and compared by taking for the 3D modeling a dimensionless height of the integration domain $H=\frac{2\pi}{k}$, periodic boundary conditions in z=*0* and z=*H* and on edges $x=\pm\pi$ and $y=\pm\pi$. An initial condition of white noise type is sufficient.

12.3.2.2. *Results*

– The Roberts flow is a dynamo with R_m^c depending on k and χ. For given values of χ and R_m, there is always a sufficiently small value of k for which the Roberts flow is a dynamo (unlike the screw dynamo). This is due to the concept of separation of horizontal scales between the flow (characteristic dimension equal to 2π) and the average magnetic field (characteristic dimension according to x and y, which is infinite).

– The time evolution of the magnetic energy is exponential in accordance with the theoretical predictions for a stationary flow.

– For χ =1, the maximum growth rate $\mathrm{Re}(p)=O(\ln(\ln R_m)/\ln R_m)$ is obtained for $kR_m^{-1/2}=O\left(\ln(R_m)^{-1/2}\right)$. The fact that $\mathrm{Re}(p)\to 0$ when $R_m\to+\infty$ confers to the Roberts flow is nature of "slow" dynamo [SOW 87] [CHI 95]. The maximum magnetic energy is confined in a layer of a thickness $O(R_m^{-1/2})$.

The growth rate according to k and R_m is represented in Figure 12.8 for χ=1.

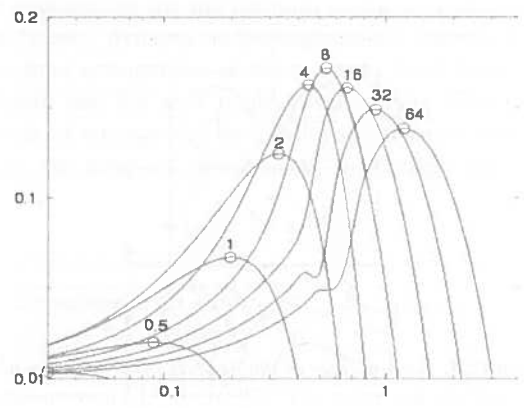

Figure 12.8. *Roberts dynamo growth rate Re(p) versus vertical wave number k, for χ=1. Each curve corresponds to $R_m=2^n$ with $n\in\{-2;-1;0;1;...;6\}$. For each value of R_m, the maximum growth rate according to k is indicated by a circle. It reaches a maximum for R_m=8 and tends towards zero for $R_m\to+\infty$ (slow dynamo)*

12.3.2.3. *Generation mechanism*

The magnetic field generation of the Roberts dynamo results mechanism of the stretching, folding or shear type.

Let us consider a magnetic field of the form $(B_x,B_y,B_z)=B_0(\cos kz,0,0)$. The stretching and folding of the magnetic field due to the flow are illustrated in Figure 12.9a in the z=0 plane.

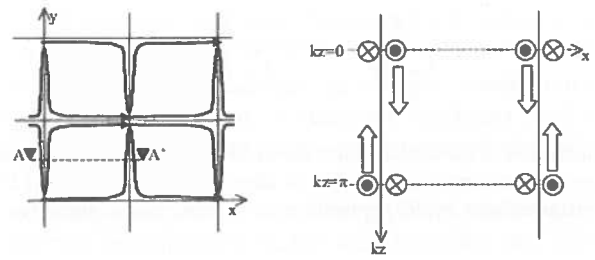

Figure 12.9. *Roberts dynamo mechanisms: (a) stretching and folding of the magnetic field in the z=0 plane; (b) sections AA': shearing of the field by vertical velocity. The white arrows represent the direction of the displacement of the field*

The field is stretched along y, consequently its intensity increases (see section 12.3.2.3). Component B_y, which appears, is of opposite direction on both sides of the borders (folding). Let us now consider the shearing according to z between two cells (section AA'). The effect of this shearing is to drag B_y in the direction of z, but in opposite directions on both sides of the border between two cells (Figure 12.9b). Consequently a field of the form $(B_x,B_y,B_z)=B_0(0,\sin kz,0)$ is generated. It is shown that this will later generate, through the same process, a field of the form $(B_x,B_y,B_z)=B_0(\cos kz,0,0)$. Consequently, the total field amplified by dynamo effect will be of the form $(B_x,B_y,B_z)=B_0(\cos kz,\sin kz,0)$.

A fundamental characteristic of the Roberts dynamo is the scale separation between the flow and the average magnetic field (spatial average in x and y). In fact, it is shown that the flow on a small scale can generate a large scale field, thanks to a mechanism known as the alpha effect [KRA 80]. This mechanism is present in most natural object dynamos. It offers an alternative and compatible explanation with the stretching, folding and shearing mechanism previously seen. Thus, an initial average field of the form $(B_x,B_y,B_z)=B_0(\cos kz,0,0)$ is deformed by the flow by forming field loops (Figure 12.10). These loops induce a current density j opposed to the field. The average magnetic field induced by this current is of the form $(B_x,B_y,B_z)=B_0(0,\sin kz,0)$. It is shown that this will later generate, through the same process, an average field of the form $(B_x,B_y,B_z)=B_0(\cos kz,0,0)$. Consequently, the total average field amplified by dynamo effect will be of the form $(B_x,B_y,B_z)=B_0(\cos kz,\sin kz,0)$.

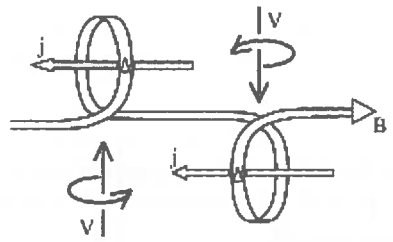

Figure 12.10. *Illustration of the alpha effect: the deformation of the average magnetic field B by vortices V generates current density j in the direction opposed to field B. This current density induces a field perpendicular to B and phase shifted in z*

It is legitimate to also consider an average magnetic field of arbitrary scale in x and y (which is not necessarily infinite). This study was undertaken within the framework of the experiment built in Karlsruhe. A liquid sodium flow goes over 52 Roberts cells. Thus, the average field has a characteristic dimension equal to the size of these 52 cells. The theoretical results obtained are noticeably different from those obtained in the ideal case of an infinite number of cells (Figure 12.11).

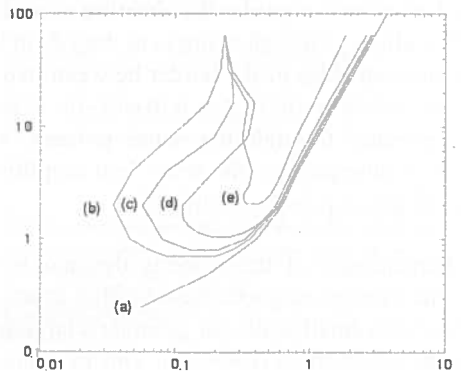

Figure 12.11. *Roberts dynamo: critical magnetic Reynolds number versus k, for χ=1. The curves correspond to an average magnetic field extending on (a) an infinity, (b) 50, (c) 32, (d) 18, (e) 8 Roberts cells*

12.3.3. *Two-scale dynamo with walls*

12.3.3.1. *Modeling*

Let us consider an integration domain made up of a square of side 2π and boundary conditions periodic in x and y. The flow is defined in dimensionless Cartesian coordinates by

$$(V_x,V_y,V_z)=(-a\sin y(1+\cos x),a\sin x(1+\cos y),Ka(1+\cos x)(1+\cos y))$$

with $K=\chi/2$ and $2a\sqrt{1+\chi^2}=1$, where χ is a screw factor. This flow consists of parallel vortices and moving in the same direction. Each vortex is included in a cell of square section and the velocity is zero on the walls of the cells. The original problem relates to a homogenous fluid in electric conductivity and magnetic permeability [PLU 99]. Walls of a different thickness and electromagnetic properties different from those of the fluid were also considered [SOT 99].

The velocity being independent of z, this problem can be still described here using a 3D or $2D^{1/2}$ ikz formulation with the same boundary and initial conditions as for the Roberts problem (section 12.3.2.1).

12.3.3.2. *Results*

– For walls with zero thickness, the results are qualitatively the same as those of the Roberts dynamo (section 12.3.2.2). However, there is a difference concerning the maximum growth rate $\mathrm{Re}(p)_{max}=O(R_m^{1/3})$ which is obtained for $k=O(R_m^{1/3})$.

– Two generation modes were identified according to k and R_m: a Ponomarenko mode and a Roberts mode.

– For walls of non-zero thickness, R_m^c depends on k, on the thickness of the walls and on the ratios of conductivity and permeability between fluid and walls.

The growth rate according to k and R_m is represented in Figure 12.12 for χ=1 and walls of zero thickness (without wall).

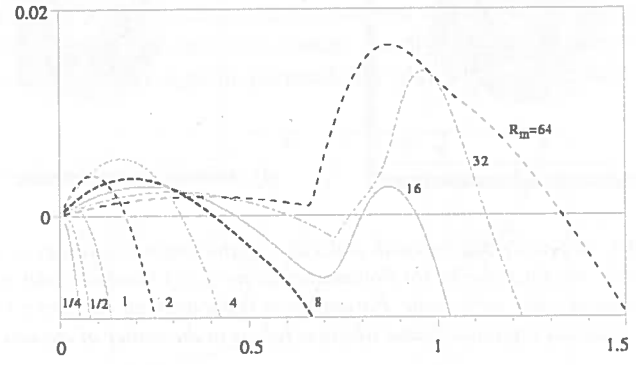

Figure 12.12. *Two-scale dynamo with walls of zero thickness: growth rate versus k for various values of R_m. The small (respectively large) values of k correspond to the Roberts (respectively Ponomarenko) mode*

12.3.3.3. *Generation mechanisms*

The generation mechanism of the two-scale dynamo with walls is again of the stretching, folding or shear type. Its originality lies in the existence of two possible dynamo modes: Roberts or Ponomarenko. Indeed, according to values of k and R_m, we observe (Figure 12.13) a magnetic energy confined in a layer either in the vicinity of the walls (Roberts mode) or inside the cells (Ponomarenko mode). In both cases, the thickness of this layer is about $O(R_m^{-1/3})$. With large R_m, the Ponomarenko mode is dominant and the solution obtained corresponds to an azimuthal mode (at the scale of one each cell) increasing with R_m (Figure 12.14).

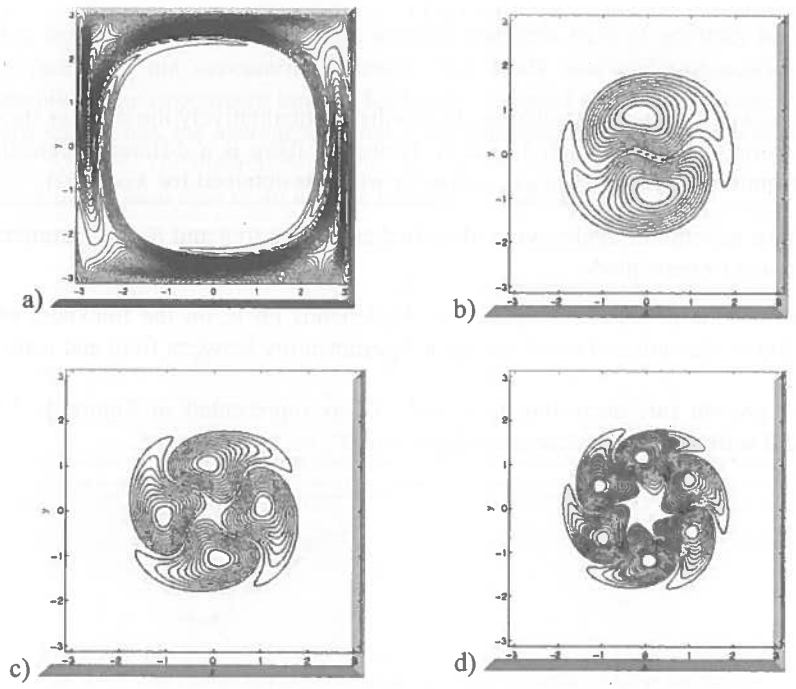

Figure 12.13. *Two-scale dynamo with walls of zero thickness: iso-values of maximum energy for the (a) Roberts, (b) Ponomarenko, m=1, (c) Ponomarenko, m=2, (d) Ponomarenko, m=3 mode. Parameter m is the azimuth mode in a local cylindrical reference frame whose origin is in the center of the cell*

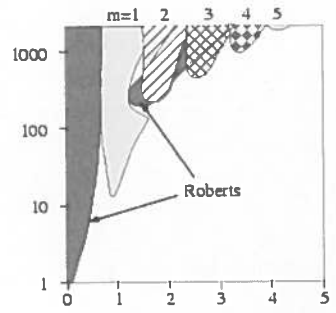

Figure 12.14. *Two-scale dynamo with walls of zero thickness: the two possible Roberts or Ponomarenko modes are represented in the plane (k, R_m^c). For the Ponomarenko mode, the local azimuthal mode m is indicated*

12.3.3.4. *Influence of walls*

At small k, the existence of non-zero thickness walls around each cell is unfavorable to the dynamo (Figure 12.15). Indeed, the mode with small k is a Roberts mode and consequently the field generation results from the cell interaction. The existence of walls slows down this interaction and R_m^c increases. At large k, the influence of walls around each cell is negligible. Indeed, the mode is then a (viscous) Ponomarenko mode and the generation takes place in the fluid, not requiring the cell interaction.

For permeability (or conductivity) walls higher than that of the fluid, the dynamo is favored at small k (Figure 12.16). The field diffusion in the walls is indeed faster and the interaction between cells is thus easier. At large k, the influence of the walls is negligible (viscous Ponomarenko mode). Lastly, as for the screw dynamo, the electric conductivity and magnetic permeability play a symmetric role.

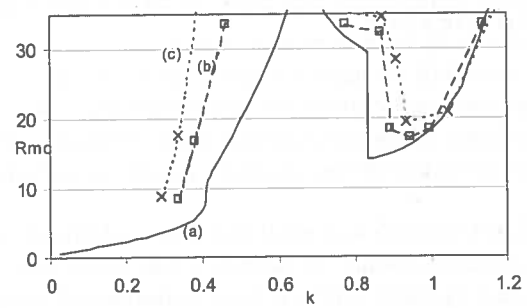

Figure 12.15. *Two-scale homogenous dynamo with walls: R_m^c versus k for various wall thicknesses. The ratio wall thickness over cell size is (a) zero, (b) 5%, (c) 10%*

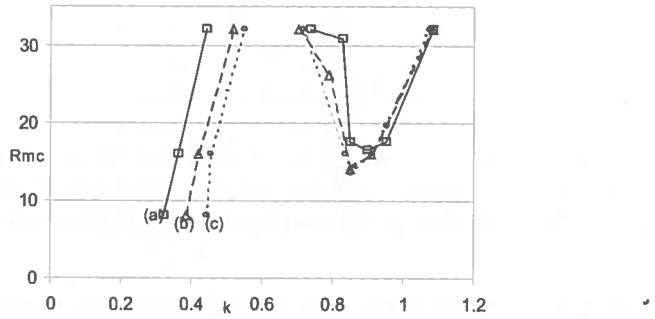

Figure 12.16. *Two-scale dynamo with walls: R_m^c versus k for a ratio wall thickness over cell size equal to 5%. The ratio of wall permeability over the fluid permeability is (a) 1, (b) 10, (c) 100*

12.3.4. *A dynamo at the industrial scale*

In 1989 and 1990, several unexpected stops occurred during the exploitation cycle of the fast breeder reactor Phénix. Each time, a furtive decrease of the power signal of the reactor was observed, engaging the security and leading to stop automatisms. Several scenarios were considered to try to explain the cause of this mysterious phenomenon. One of them was based on the existence of a mechanical instability caused by a dynamo effect in the reactor. The core of the reactor is actually traversed by liquid sodium at high speed with a flow geometry similar to the two-scale dynamo with walls thus favorable to a spontaneous amplification of magnetic field. In addition, the walls of the cells of the core being built with ferromagnetic materials, the efforts exerted by the interaction of the field and the currents in sodium were sufficient to generate the mechanical instability necessary to trigger the security stops. Thus, a dynamo effect was probably observed in an indirect way in the core of a FBR.

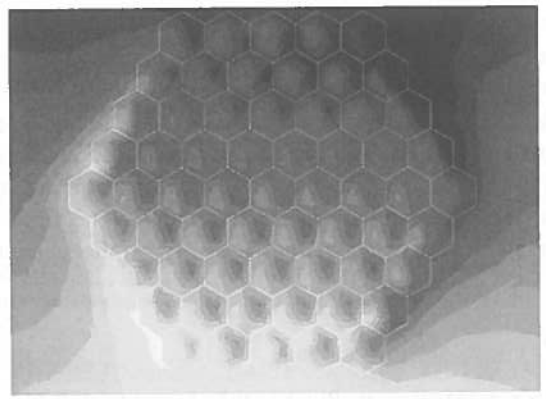

Figure 12.17. *Iso-value Bz in a horizontal section of an FBR core. The clear (bold) color indicates a positive (negative) value of Bz*

The result of an EF3D calculation is presented in Figure 12.17 where the iso-values of the vertical component of the magnetic field in a horizontal section of the core of the reactor are represented. For this calculation, the core consists of 61 cells of hexagonal section. The flow traversing each cell is a viscous screw flow. The main interest of this figure is that it shows a double organization of the magnetic field. The field is organized in a double helix at the scale of each cell as in Figure 12.2 and in accordance with the screw dynamo. The field is also organized in a double helix at the scale of the core. This double organization of the field is characteristic of a two-scale dynamo such as that also observed in the Karlsruhe experiment.

12.4. Modeling of the dynamic problem

The dynamic problem (modeling of the induction and Navier-Stokes equation) was formulated and modeled by the finite element method [BEN 99] [BEN 01] in the case where the whole integration domain is homogenous in conductivity and permeability. The tests carried out present a magnetic Reynolds number too low to obtain a dynamo. The formulation uses the primary variables: speed, pressure and magnetic field. The originality of the method relies on the coupling strategy between the resolution of the Navier-Stokes equations and the induction equation.

In addition, it should be noted that there is a dynamo benchmark in spherical geometry which was tested and validated by various research teams [CHR 01]. Generally, the space discretization used is of the spherical harmonics type for the latitudinal and longitudinal dependences. The discretization in the direction of the radius is of the spectral or finite differences type. The use of spherical harmonics is

naturally suggested by the spherical geometry of the integration domain. In addition, it has the advantage of being able to select a reduced number of harmonics (as far as this selection can give reasonable results). The calculation time can thus be considerably reduced (as for the $2D^{1/2}$ and $1D^{1/2}$ resolutions described in section 12.2.2). In comparison, the 3D finite element method does not *a priori* allow an economical resolution to be chosen unless a time adaptive mesh is used (allowing us to have a refined mesh where the scales are similar). The finite element method could also become more advantageous for massively parallel calculations.

12.5. References

[ALE 00] ALEMANY A., MARTY P., PLUNIAN F., SOTO J., "Experimental investigations of dynamo action in the secondary pumps of the FBR Superphénix", *J. Fluid Mech.*, no. 403, pp. 263-276, 2000.

[BEN 99] BEN SALAH N., SOULAIMANI A., HABASHI W.G., FORTIN M., "A conservative stabilized finite element method for the magnetohydrodynamic equations", *IJNMF*, vol. 29, no. 535, 1999.

[BEN 01] BEN SALAH N., SOULAIMANI A., HABASHI W.G., FORTIN M, "A finite element method for the magnetohydrodynamic", *Comp. Meths. Appl. Mech. Engrg.*, 2001.

[BER 07] BERHANU M. et al., "Magnetic field reversals in an experimental turbulent dynamo", *Eur. Phys. Lett.* 77 (5), 59001 2007.

[BIR 89] BIRO O., KURT P., "On the use of the magnetic vector potential in the finite element analysis of three dimensional eddy currents", *IEEE Trans. Mag.*, vol. 25, no. 4, 1989.

[BUS 96] BUSSE F.H., MULLER U., STIEGLITZ R., TILGNER A., "A two-scale homogenous dynamo: an extended analytical model and an experimental demonstration under development", *Magnetohydrodynamics*, vol. 32, pp. 235-248, 1996.

[CHI 95] CHILDRESS S., GILBERT A.D., *Stretch, Twist, Fold: The Fast Dynamo*, Springer, 1995.

[CHR 01] CHRISTENSEN U.R., AUBERT J., CARDIN P., *et al.*, "A numerical dynamo benchmark", *Phys. Earth Planet. Inter.*, vol. 128, 2001.

[COX 69] COX A., "Geomagnetic reversals", *Science*, vol. 163, pp. 237-245, 1969.

[CSE 82] CSENDES Z.J., WEISS J., HOOLE S.R.H., "Alternative vector potential formulation of 3D magnetostatic field problems", *IEEE Trans. Mag.*, vol. 18, pp. 367-372, 1982.

[GAI 76] GAILITIS A., FREIBERGS J., "To the theory of a helical MHD-dynámo", *Magnetohydrodynamics*, vol. 12, pp. 127-129, 1976.

[GAI 00] GAILITIS A., LIELAUSIS O., DEMENT'EV S., *et al.*, "Detection of a flow induced magnetic field eigenmode in the Riga dynamo facility", *Phys. Rev. Lett.*, vol. 84, pp. 4365-4368, 2000.

[GAI 01] GAILITIS A., LIELAUSIS O., PLATACIS E., *et al.*, "Magnetic field saturation in the Riga dynamo experiment", *Phys. Rev. Lett.*, vol. 84, pp. 4365-4368, 2000.

[GIL 88] GILBERT A., "Fast dynamo action in the Ponomarenko dynamo", *GAFD*, vol. 44, p. 241, 1988.

[GUE 07] GUERMOND J.L., LAGUERRE R., LEORAT J., NORE C., "An interior Penalty Galerkin Method for the MHD equations in heterogeneous domains", *J. Comp. Physics* 221, 349, 2007.

[HID 79] HIDE R., "Dynamo theorems", *GAFD*, vol. 12, pp. 171-176, 1979.

[KOL 61] KOLM H.H., MAWARDI O.K., "Hydromagnet: a self-generating liquid conductor electromagnet", *J. of Applied Phys.*, vol. 32, no. 7, p. 1296, 1961.

[KRA 80] KRAUSE F., RÄDLER K.-H., *Mean Field Magneohydrodynamics and Dynamo Theory*, Akademie-Verlag and Pergamon, 1980.

[LAG 06] LAGUERRE R., NORE C., LEORAT J., GUERMOND J.L., "Effects of conductivity jumps in the envelope of a kinematic dynamo flow", *CR Mécanique* 334, 593, 2006.

[LEO 80] LÉORAT J., POUQUET A., FRISCH U., "Turbulence MHD développée et génération de champ magnétique", *J. Phys.*, vol. 41, pp. 359-369, 1980.

[MAR 06] MARIE L., NORMAND C., DAVIAUD F., "Galerkin analysis of kinematic dynamos in the von Karman geometry", *Phys. Fluids* 18, 017102, 2006.

[MAS 84] MASSÉ P., "Modeling of continuous media methodology and computer-aided design of finite element programs", *IEEE Trans. Mag.*, vol. 20, no. 5, pp. 1885-1890, 1984.

[MER 95] MERRILL R.T., MCFADDEN P.L., "Dynamo theory and paleomagnetism", *J. Geophys. Res.*, vol. 100, pp. 317-326, 1995.

[MOF 78] MOFFATT H.K., *Magnetic Field Generation in Electrically Conductive Fluids*, Cambridge University Press, New York, 1978.

[MOF 89] MOFFATT H.K., "Stretch, twist and fold", *Nature*, 341, 1989.

[MON 06] MONCHAUX R. *et al.*, "Generation of magnetic field by a turbulent flow of liquid sodium", *Phys. Rev. Lett.* 98, 044502, 2006.

[MOR 90] MOREAU R., *Magnetohydrodynamics*, Kluwer Acad. Publ., Dordrecht/Boston/ London, 1990.

[PAR 66] PARKER R.L., "Reconnexion of lines of force in rotating spheres and cylinders", *Proc. Roy. Soc.*, A291, pp. 60-72, 1966.

[PEY 07] PEYROT M., PLUNIAN F., NORMAND C., "Parametric instability of the helical dynamo", *Phys. of Fluids*, 19, 054109, 2007.

[PLU 95] PLUNIAN F., ALEMANY A., MARTY PH., "Influence of MHD parameters on electromagnetic self-excitation in the core of a FBR", *Magnetohydrodynamics*, vol. 31, 4, 1995.

[PLU 96] PLUNIAN F., Etude de l'effet dynamo dans le coeur du réacteur Phénix, Thesis INPG, 1996.

[PLU 96] PLUNIAN F., MASSÉ PH., "An optimal preconditionned scheme for finite element modeling of kinematic MHD dynamo effect", *Proc. of Eccomas 96*, France, 1996.

[PLU 98] PLUNIAN F., ALEMANY A., MARTY PH., MASSÉ PH., "Direct numerical modeling of kinematic dynamo effect. Application to the geometry of the core of the French fast breeder reactor Phénix", *Progress in Astronautics and Aeronautics*, AIAA 182, pp. 537-550, 1998.

[PLU 99] PLUNIAN F., MARTY PH., ALEMANY A., "Kinematic dynamo action in a network of screw motions. Application to the core of a fast breeder reactor", *J. Fluid Mech.*, vol. 382, pp. 137-154, 1999.

[PLU 02] PLUNIAN F., RÄDLER K.-H., "Harmonic and subharmonic solutions of the Roberts dynamo model. Application to the Karlsruhe experiment", *Magnetohydrodynamics*, 2002.

[PLU 02] PLUNIAN F., RÄDLER K.-H., "Subharmonic dynamo action in the Roberts flow", *Geophys. Astr. Fluid. Dyn.*, vol. 96, no. 2, pp. 115-133, 2002.

[PON 73] PONOMARENKO Y.B., "On the theory of hydromagnetic dynamo", (Zh. Prikl. Mekh. Tekhn. Fiz. USSR, 6, 47-51), *J. Appl. Mech. Tech. Phys.*, vol. 14, pp. 775-779, 1973.

[PRI 82] PRIEST E.R., "Solar magnetohydrodynamics", *Geophys. and Astr. Monographs*, D. Reidel Pub. Comp., 1982.

[PRO 79] PROCTOR M.R.E., "Necessary conditions for the MHD Dynamo", *GAFD*, vol. 14, pp. 127-145, 1979.

[RAD 95] RÄDLER K.-H., "Cosmic Dynamos", *Rev. Mod. Astron.*, vol. 8, pp. 295-321, 1995.

[RAD 98] RÄDLER K.-H., APSTEIN E., RHEINHARDT M., SCHÜLER M., "The Karlsruhe dynamo experiment – a mean field approach", *Studia geoph. et geod.*, vol. 42, pp. 224-231, 1998.

[ROB 72] ROBERTS G.O., "Dynamo action of fluid motions with two-dimensional periodicity", *Phil. Trans. R. Soc.*, London, A271, 411, 1972.

[ROB 92] ROBERTS P., SOWARD A.M., "Dynamo theory", *Ann. Rev. Fluid Mech.*, Vol. 24, pp. 459-512, 1992.

[SCH 92] SCHMITT D., "The solar dynamo", *IAU Symposium*, no. 157, Potsdam, 1992.

[SOT 98] SOTO J., PLUNIAN F., MASSÉ PH., "A finite element-spectral formulation for the kinematic MHD dynamo problem", *Proc. of Eccomas 98*, Greece, 1998.

[SOT 99] SOTO, Etude cinématique de l'effet dynamo en milieu non homogène. Application aux réacteurs à neutrons rapides, Thesis, INPG, 1999.

[SOW 87] SOWARD A.M., "Fast dynamo action in a steady flow", *J. Fluid Mech.*, vol. 180, pp. 267-295, 1987.

[STI 01] STIEGLITZ R., MÜLLER U., "Experimental demonstration of a homogenous two-scale dynamo", *Physics of Fluids*, vol. 13, pp. 561-564, 2001.

[VAL 93] VALET J.P., MENADIER L., "Geomagnetic field intensity and reversals during the past four million years", *Nature*, vol. 366, pp. 234-238, 1993.

[WEI 66] WEISS N.O., "The expulsion of magnetic flux by eddies", *Proc. Roy. Soc.*, A293, pp. 310-328, 1966.

[WEI 94] WEISS N.O., "Solar and stellar dynamos", in *Lectures on Solar and Planetary Dynamos*, Proctor M.R.E. and Gilbert A.D. (eds.), Camb. Univ. Press, New York, 1994.

[ZEL 83] ZELDOVITCH YA. B., RUZMAIKIN A.A., SOKOLOFF D.D., *Magnetic Fields in Astrophysics*, Gordon and Breach Science Publishers, New York, 1983.